Jurnal Tribologi 38 (2023) 49-68

MYTRIBOS Malaysian Tribology Society

Jurnal Tribologi

Website : jurnaltribologi.mytribos.org e-issn: 2289-7232

Using Finite Element simulation to investigate the effect of cutting edge radius on burr formation for inclined dimple milling operation

Mohd Ali Hanafiah Shaharudin *, Ahmad Razlan Mohd Yusoff

Fakulti Teknologi Kejuruteraan Pembuatan & Mekatronik, Universiti Malaysia Pahang Al-Sultan Abdullah. 26600 Pekan Pahang, MALAYSIA.
* Corresponding author: alihanafiah@ump.edu.my

KEYWORDS

Micro-milling
Burr formation
Finite element approach
Tool cutting edge
Aluminium alloy
Dimple milling

ABSTRACT

In any mechanical cutting operation including micro-milling, burr formation is unavoidable due to the plastically deformed materials generated from the cutting and shearing phenomenon. Compared to macro milling, the size ratio between burr and micro-milling profile is extremely large making the removal process extremely challenging. Due to the challenge, this paper presents the investigation of critical factors in burr formation such as tool cutting edge radius, Rc using the finite element (FE) approach. The first part of the investigation consists of the validation of the FE simulation results with the experimental by comparing the generated cutting force, and the second part focused on the virtual experiment on the investigation of tool cutting edge radius to the burr formation on the machined dimple profile. In the simulation of inclined dimple milling, the 3D model of solid carbide (WC) ball end mill (BEM) tool contact with the round Aluminum Alloy 6061-T6 specimen model at 45° inclination angle to form the dimple profile and the characteristic of the burr profile measured directly on the deformed specimen model. Based on the results, it was found the cutting edge radius, directly proportional to the cutting force and significantly influence the burr formation in inclined dimple milling.

Received 1 August 2022; received in revised form 9 November 2022; accepted 22 March 2023.
To cite this article: Shaharudin and Mohd Yusoff (2023). Using finite element simulation to investigate the effect of cutting edge radius on burr formation for inclined dimple milling operation. Jurnal Tribologi 38, pp.49-68.

1.0 INTRODUCTION

Micro dimple profile is designed to serve the function of reducing the coefficient of friction in a way where it reduces the contact area between two contact surfaces, generates a hydrodynamic pressure (in certain shape and configuration), and acts as an oil reservoir during surface in motion as well as pits for worn particle/debris to accumulate (Pratap & Patra, 2018). This could only be achieved through high-precision fabrication processes such as micro-milling that are capable of machine the intended dimple profile and shape at micro level. At this machining level, any dimensional shape or profile discrepancy due to machining process such as surface roughness, burr, build-up edge etc. could ruin the designated dimple functions as well as lead to increased manufacturing costs due to difficulties in accessibility and tight tolerances in micro components.

As far as surface roughness is concern, the conventional method of milling with Ball End Mill (BEM) tool at right angle with the workpiece had experience with a coarse machined surface due to a phenomenon so call "rubbing effect" where low cutting speed at the tool tip has tend the tool tip to rub the surface rather than cut. So due to the problem, inclined milling is introduced where the technique (Figure 1) adopts the use of BEM tool to machine a surface contour at a certain angle, θ to improve the surface roughness of machined surface by BEM tool. Varying the inclined angle, Θ shifting the contact point of the BEM tool along the latitude of the ball end sphere to avoid the rubbing effect at the tip of the BEM (Wojciechowski & Mrozek, 2017). Using this technique, the BEM tip rubbing effect that deteriorates the machined surface can be minimized and improved the surface finish (Pratap & Patra, 2018).

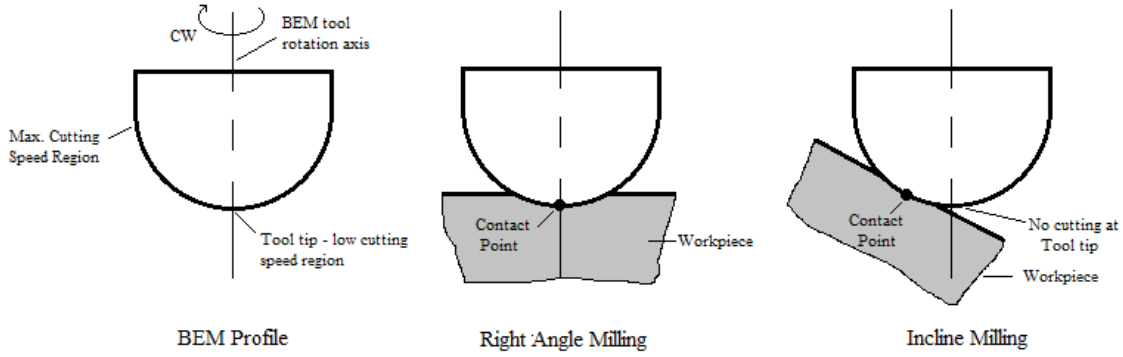

Figure 1: Illustration of cutting speed variation along its radial direction and interaction between contact point of BEM and workpiece positions.

1.1 Burr Formation

In mechanical cutting operation, stress induces in the elastic-plastic region within the workpiece materials not only deforms the work materials to form the chip (Zhang et al., 2019) but also leads to burr formation on the machined profile. Unlike machined chips that get separated away during cutting, the burr is an edge imperfection in the form of protruding, ragged excess material remaining along part's edges of the machined profile. In previous research work done on the burr formation in the micro-milling process (W. Chen et al., 2018; Z. Chen et al., 2021; Luo et al., 2008; Saptaji et al., 2012; Zhang et al., 2019)concluded the most critical factors such as machining parameters, geometry of the cutting tool, tool and workpiece material, tools, and cutting condition. The machining burr is classified differently by different researchers either

based on formation mechanism, burr shapes or locations. According to the location definition (Figure 2), there are three types of machining burrs commonly formed during machining operation: namely, Top Burr, Entrance Burr, and Exit Burr (Kiswanto et al., 2014) .

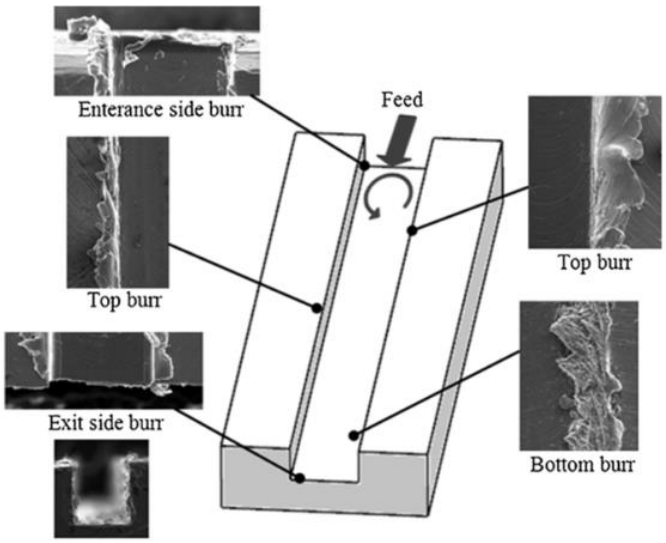

Figure 2: Classification of formed burr base on location in slot milling operation (Kiswanto et al., 2014).

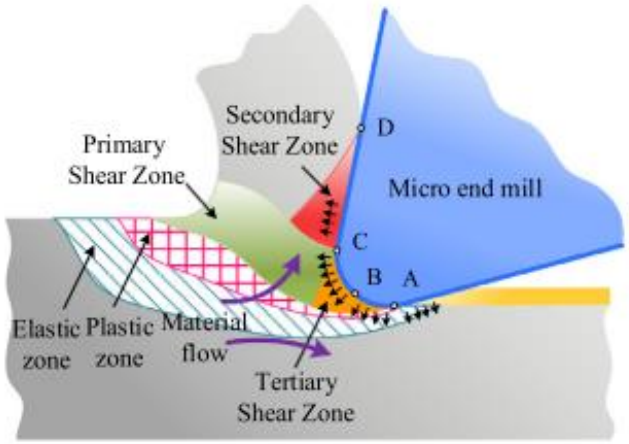

Figure 3: Formation of stress zone due to force exert by the cutting edge radius, R_c during machining operation (Zhang et al., 2019).

Among the critical factors, cutting edge radius, R_c is one of the interesting tool geometries factors to be studied. The tool cutting edge radius, R_c is known to be directly in contact with the workpiece and exert force inducing the stress within the workpiece and formed the chip as show in figure 3. In a recent study, size of the cutting edge will significantly affect chip formation and

thermo-mechanical load thus, it also affects changes in cutting force (Vipindas et al., 2018) . Based on this study (Lv et al., 2020) indicated that cutting edge radius, R_c remarkably significant to the cutting performances where an increase of cutting edge radius, R_c will increase the cutting force directly.

Unlike other milling processes, burr formation in an inclined dimple milling technique is quite different due to the orientation of the tools and the workpiece as well as the dimple profile itself. Based on the rotational direction and the toolpath, the burr tends to build up at the edge of the dimple (Figure 4) somewhere close to tool exit region (Pratap & Patra, 2018). It could be classified as an exit burr formed due to the chip stretch-up and break-off from the parent materials during the cutting process.

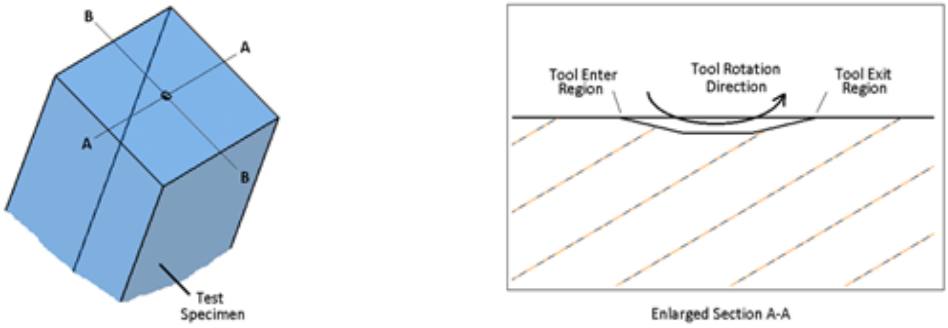

(a) (b)

Figure 4: Burr formation tendency at the edge of the dimple profile/ exit region during cutting operation (a) Isometric view of workpiece, (b) Cross-section view of machined dimple profile.

1.2 Friction in Metal Cutting

Friction at tool-chip interface plays a significant role in dictating the cutting forces, temperature, and tool wear (Kılıçaslan, 2009). Due to that, a lot of research work focused on determining the right friction model to represent the real behaviors of the process. In metal cutting, the dual zone rake face contact model is the most common model used to define the characteristic of friction force that divides the rake face into two regions: sticking and sliding (Zorev, 1963). It is also supported by (Usui & Takeyama, 1960) who measured the distribution of the shear stress (τ) and the normal stress (σ) on the rake face of the tool have found that the shear stress remains constant over about half of tool-chip contact length (point A to B) then decrease and reach zero at point C where the chip leaves contact with the tool (Figure 5a). Meanwhile, the normal stress was found to decrease exponentially and reach zero from the cutting edge to point C.

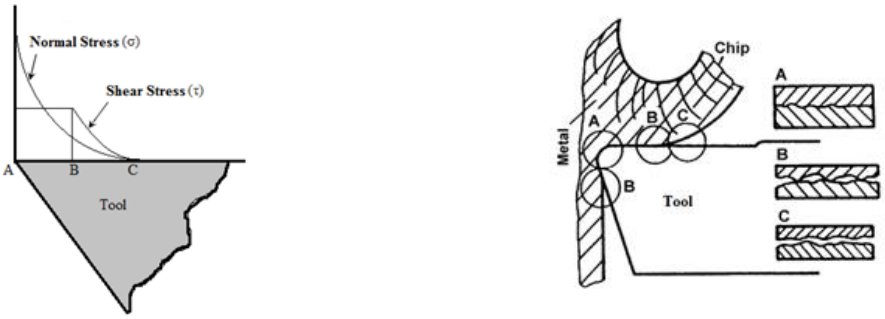

(a) (b)

Figure 5: Contact mechanic at tool-chip interface (a)Normal and Shear stress distribution over the tool rake surface (Kılıçaslan, 2009) and (b) surface contact condition at tool-chip interface (Childs, 2006).

Throughout the length of AB (Figure 5a) where normal stress is sufficiently high and the ratio of actual contact area to the total area approaches unity (Figure 5b) causing the work material tends to adhere to the rake face of the tool. This region is called the sticking region where the plastic deformation occurs to form the chip. In this region, the coefficient of friction is not constant, but it depends on the magnitude of the normal load, and it is found that the value of the coefficient of friction in this region is lower than the value under sliding friction conditions. While at the length from B to C, where the formed chip loses contact with the rake face of tool, the ratio of actual contact area to the total area ratio is less than unity, so coefficient of friction is constant, and sliding friction occurs. The measured coefficient of friction in metal cutting is an average value based on both regions. Any changes in cutting conditions that may change lengths AB and BC will change the value of coefficient of friction (Kılıçaslan, 2009).

Based on literature work summarize that all previous research work done already cover almost every aspect on the burr formation in the micro-milling process including the critical factor, optimization of machining parameters and tool geometry, burr reduction method and many more. But recently inclined milling is become trending and extensively being applied to fabricate a dimple structure surface and yet lack of specific analysis on burr formation in an inclined dimple milling operation. Due to that, this research work tries to enlighten the formation of burr in micro dimple milling based on Finite Element Analysis (FEA) approach using DEFORM 3D software.

2.0 SIMULATION WORK

The inclined milling simulation is a finite element analysis approach that was done to simulate the cutting phenomenon, deformation of the work materials as well as observing the burr formation in incline dimple milling operation. Other than that, the simulation also attempts to simulate the effect of the cutting-edge radius, R_c on the burr formation in inclined dimple milling operation. The simulation of inclined milling will be conducted using DEFORM-3D software (version 10, Scientific Forming Technologies Corporation, Columbus, Ohio). As shown in flowchart figure 6, the simulation will simulate the inclined dimple milling based on the coefficient of friction, μ gained from the literature. The results then will be validated with the actual experimental work done by previous researcher (Graham et al., 2014) and the summary of

experimental work parameters are tabulated as shown in table 1. With the satisfied coefficient of friction, μ the simulation of the effect of "cutting edge radius" will be carried out and analyzed.

The DEFORM-3D simulation process consists of two phases namely phase 1; pre-processor and phase 2; post-processor. In the phase 1 or the pre-processor parts, the 3D models, meshing, motion and speed parameters, and boundary conditions are assigned and due to validation purposes, the simulation input parameter will be set up as close as possible with the actual experimental work done. While the phase 2 or the post-processing phase where simulation and analysis of results are performed.

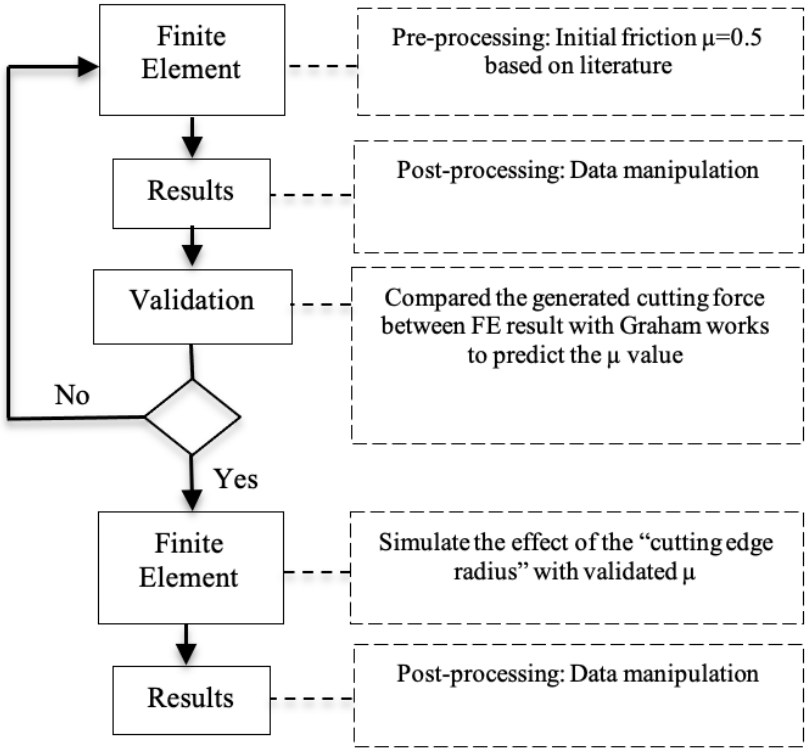

Figure 6: Flowchart of the research work to simulate the inclined dimple milling.

Table 1: Parameters applied in the experimental work by (Graham et al., 2013).

Parameters	**Value**
Tool size	Ø500μm
Materials	Tool: Carbide (WC), Workpiece: Aluminum Alloy 6061-T6
Incline Angle	45°
Spindle Speed	500 rpm
Feed	2.5 mm/s
Dimple Depth	7 μm

2.1 Phase 1: Pre-processing

In any simulation, the crucial element properties for both tool and specimen such as mechanical and thermal properties need to be defined to ensure the accuracy of the FEA simulation. This material's property values govern the physical law and affecting directly to the computational results of the simulation. Due to that, the value of the mechanical and thermal properties for both BEM tool and the workpiece is carefully determined and summarized in Table 2.

The material properties of workpiece are set to Aluminum (AL 6061T6) cylinder whereas the BEM tool is modeled as Tungsten Carbide, and the summary of both material properties as shown in table 2. The size of the workpiece cylinder is selected based on the software developer guideline that suggested the workpiece model must be constructed at least 20 % larger than the cutting tool diameter (>500 m). Meanwhile, The BEM tool was modeled only at the spherical parts to minimize the number of mesh elements as shown in figure 7 below. The BEM tool is inclined about $\theta = 45°$ along Y-axis and the workpiece lies horizontally.

Table 2: Summary of mechanical properties of BEM tool and the work piece materials applied to simulation work.

Properties	**Ball End Mill Tool**	**Test Specimen**
Materials	Coated Tungsten Carbide (WC)	Aluminum Alloy (AL6061-T6)
Density (kg m^{-3})	14500	2730
Poisson Ratio	0.21	0.33
Elastic Module (MPa)	612000	68900
Yield Strength (MPa)	-	276
Ultimate Tensile Strength (MPa)	370	310
% Elongation	-	18
Specific Heat (J kg^{-1} K^{-1})	337	896
Thermal Conductivity (W m^{-1} K^{-1})	110	187

During simulation, the toolpath of BEM tool consists of multiple motions mainly positioning, cutting, and retracting. Initially, the BEM tool will move to the feed position at a rapid feed rate, followed by the cutting movement in the Z-axis direction (at predetermined feed rate and depth) where the tool plunges directly to the inclined surface feed rate. The parameters imposed to the simulation work are replicating the experimental work done as tabulated in table 1.

In pre-processing setup, the test workpiece movement and rotation were restricted in all directions (X, Y, and Z.). Whereas the ball end mill tool was allowed to be rotated around the tool axis (clockwise) and move in the Z-axis direction (feed direction) with predetermined feed speed to simulate the cutting action (figure 7). The BEM tool was treated as a rigid object (assumed to be no shape deformation occurred during the cutting operation), and the test specimen was considered as a plastic object (deformed according to the governing physical law).

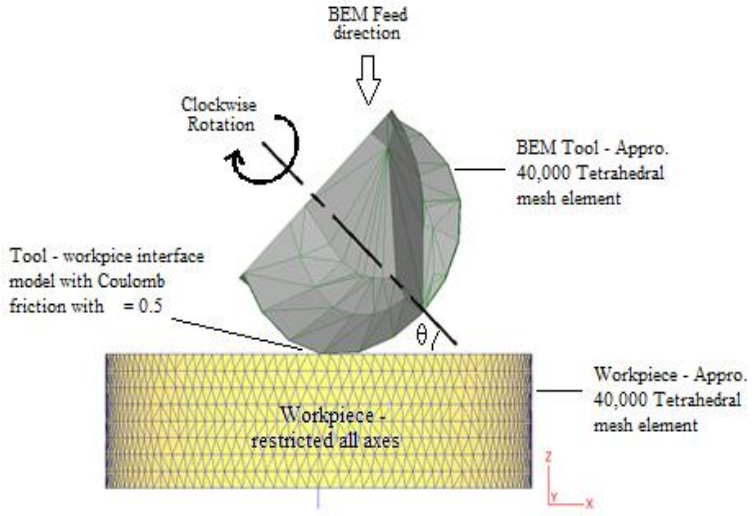

Figure 7: BEM tool and workpiece orientation and parts of pre-processing setup applied to the simulation.

In the present simulation works, Lagrangian Incremental method was used to simulate the cutting phenomenon between the BEM tool and the aluminum workpiece. For the material model, DEFORM is employing the power law method to define materials flow stress. The model and applied to both tool and workpiece since it's a well-known model that is capable of predicting the material movement and deformation accurately. In the model the plastic flow stress during the cutting process is formulated as:

$$\overline{\sigma} = c\,\overline{\varepsilon}^{\,n}\,\dot{\overline{\varepsilon}}^{\,m} + y \tag{1}$$

Where $\overline{\sigma}$, is the materials flow stress, $\overline{\varepsilon}$, is effective plastic strain, $\dot{\overline{\varepsilon}}$, effective strain rate, c, material constant, n, strain exponent, m, strain rate exponent and y, initial yield value.

In the DEFORM software, the flow stress, $\boldsymbol{\sigma}_{\text{flow}}$ of the AA 6061 T6 materials is characterized as temperature, strain, and strain rates dependent as shown in graph figure 8 below.

For the meshing, benchmarking was done with previous research (Bolar & Joshi, 2014; Z. Chen et al., 2015; Mohruni et al., 2019; Tamizharasan & Senthilkumar, 2012; Yıldız et al., 2020) preferred the number of relative meshing elements between 30,000 to 40,000 with Tetrahedron element shape for both tool and workpiece as summarized in table 3. The element's size ranging between minimum to maximum was 0.003 mm and 0.03 mm respectively. Localize meshing methods are also applied to both tool and workpiece where a specific portion of the object has a finer mesh size, rather than the entire part. At the cutting-edge area on the BEM tool and machined surface of the workpiece, local meshing with a size ratio of 0.1 is applied where the size of the elements inside the pre-selected area are 10 times finer than the outside elements.

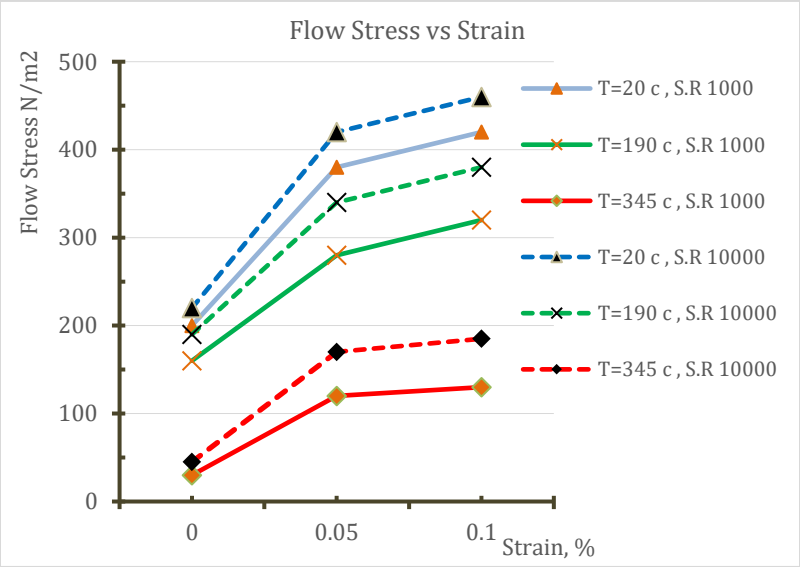

Figure 8: Characteristic of Flow stress, σ_{flow} of the AA 6061 T6 materials dependent on temperature, strain, and strain rates.

In DEFORM software, the interface between the tool-chip is modeled to have contact friction and this friction significantly affects the simulation especially the cutting force since the frictional energy will convert into heat. The friction conditions at the tool-chip interface are modeled differently according to its deformation regions. In the sliding region, the friction is modeled as Coulomb friction where force of friction is proportional to the normal load and is independent of the contact area. Coulomb's model, was extensively used to model manufacturing processes due to its simplicity and mathematically formulate as follows:

Coulomb friction, $$F_s = \mu\, p \quad (2)$$

Where F_s frictional force, μ friction coefficient, p interface normal load

While at the "sticking region", the friction at the tool-chip interface modeled with the constant-friction model where the frictional force is considered equal to the product of a friction factor m and shear flow stress k of the weaker material. In the constant-friction model, the friction force does not depend on the normal load. Hence, the model is suited to carry out the analysis of metal forming processes using an upper bound method. In this method, the power needed for the plastic deformation and overcoming the friction is calculated where the total power, based on the assumed velocity field, is always higher than the actual power.

Shear friction, $$F_s = m\, k \quad (3)$$

Where F_s frictional force, m friction coefficient, k shear yield stress

Even though friction is known to exist at the tool-chip contact interface, the determination of the actual value of friction is difficult, especially in micromachining operations due to micro size tool. Based on previous research done (Davoudinejad et al., 2017; G. Li et al., 2021) on the

simulation of Aluminum Alloy 6061-T6, preferred the Coulomb friction model for their simulation work, so in the present simulation work the Coulomb friction model will employ the same value of μ=0.5.

Table 3: Summary of meshing parameters and boundary condition applied in simulation.

	Ball End Mill Tool	**Workpiece**
Element Type	Tetrahedral Element	Tetrahedral Element
No. of Element	Approx. 40,000	Approx. 40,000
Meshing Size (Min. - Max)	0.003- 0.03mm	0.003- 0.03mm
Local Mesh Ratio	None	0.1at chip formation area
Degree of Freedom	2 (Rotation about tool-axis & movement -Z-axis)	0
Shape Model	Rigid	Plastic
Initial Temperature	30°C	30°C
Friction Model	Coulomb Friction, μ = 0.5	Coulomb Friction, μ = 0.5

The 3D model of BEM tool is designed using commercial designing software based on the derived cutting-edge curves plotted using MATLAB software. The BEM model was constructed as two flutes with a 30° helix angle, and a summary of the tool geometry design is tabulated in table 4 below. The derivations of the cutting edge are based on the 3D cartesian coordinate system of the intersection curve between the spherical surface and the helical surface (Ji et al., 2015) as shown in figure 9 where the center of the spherical, O is the origin. Based on the intersection definition, thus any point on the cutting edge of the BEM at the spherical region can be expressed by the following equations 4-6

$$x = R\sqrt{1-(c\varphi)^2}.cos\varphi \quad (4)$$

$$y = R\sqrt{1-(c\varphi)^2}.sin\varphi \quad (5)$$

$$z = Rc\varphi \quad (6)$$

$$c = \frac{1}{tan\varphi} \quad (7)$$

Where R, tool radius, φ , parameter angle for $0 \leq \varphi \leq 2\pi$, c, helix parameter

Table 4: Details of BEM tool tip geometry parameter of ball end mill tip applied to the 3D model.

Tool Geometry	**Value**
Diameter	Ø0.5 mm
Clearance Angle	9°
Rake Angle	10°
Helix's Angle	30°
Cutting-edge Radius	5, 10, 20, 30μm

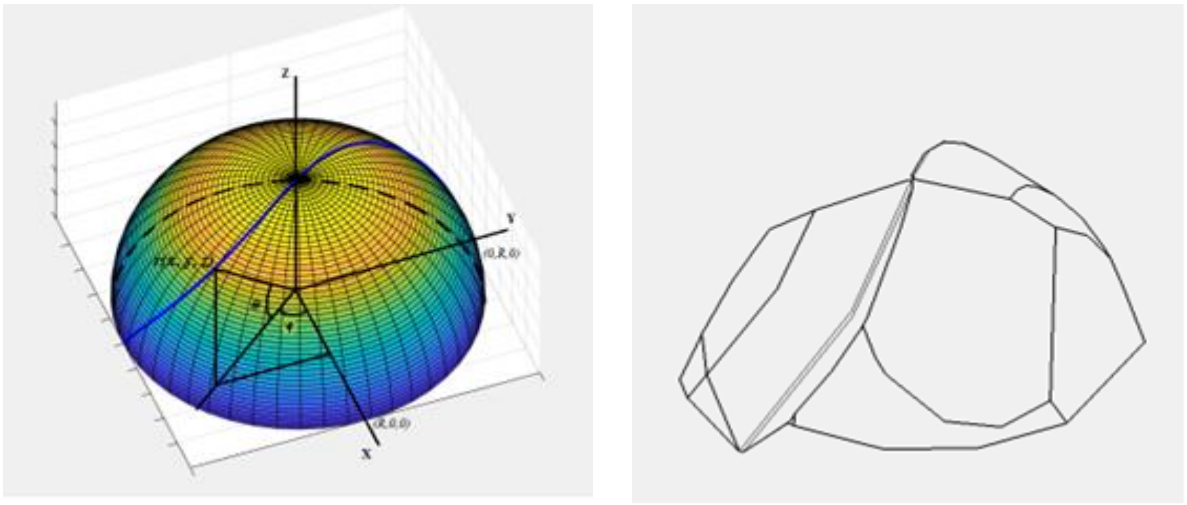

(a) (b)

Figure 9: Cutting tool geometry (a) Cartesian Coordinate used for cutting edge with helix angle of 30° plotting using MATLAB (b) BEM tip designed in CATIA software.

2.2 Phase 2: Post-processing

In the phase 2 of the simulation or the "post processing", the simulation results will be analyzed thoroughly the cutting phenomenon based on the research objectives. In general, the analysis will be carried out on the:

1. Cutting force Analysis– to compare the simulated cutting force with the actual cutting force generated in the experimental work by (Graham et al., 2014) and validate the value of the coefficient applied in the simulation.
2. Burr Formation Analysis -to observe the burr morphology, characteristic and burr size measurement.

In the present simulation work, the result of the simulation will be validated with an actual experiment conducted by a previous researcher (Graham et al., 2013). In the experiment, the designated experimental work is means to capture the milling cutting force in all axes exerted on the workpiece by the tool during cutting operation as well as to observe physically in terms of size and depth of the machined dimple profile. In fact, the parameter settings in this simulation are set up as close as possible to the experiment scenario to ensure the FEA simulation result and the experimental result closely match each other within the acceptable error.

3.0 RESULTS AND DISCUSSION

3.1 Validation Result

In the simulation results, the force exerted by the tool tips has been plotted against spindle rotation angle. Figure 10 shows that the force in x, y and z-axis with a magnitude of 0.1, 0.33 and 0.63 N respectively with highest force exerted by the y-axis and the lowest force exerted by the x-axis. Based on this, results from the inclined dimple milling simulations find good agreement with the captured cutting force data in the dimple cutting experimental of Aluminum Alloy 6061-T6 under incline milling configuration with the same cutting conditions (Graham et al., 2013) in

terms of the rank of force (Figure 11). However, in terms of magnitude as compared to the experiment result shows that the simulation results underestimate the cutting force in all axes. As comparison with the simulation results, the force captured by the experimental work in x, y and z-axis approximately 0.3, 0.8 and 1.4N respectively with error percentage almost 50% in all axes direction.

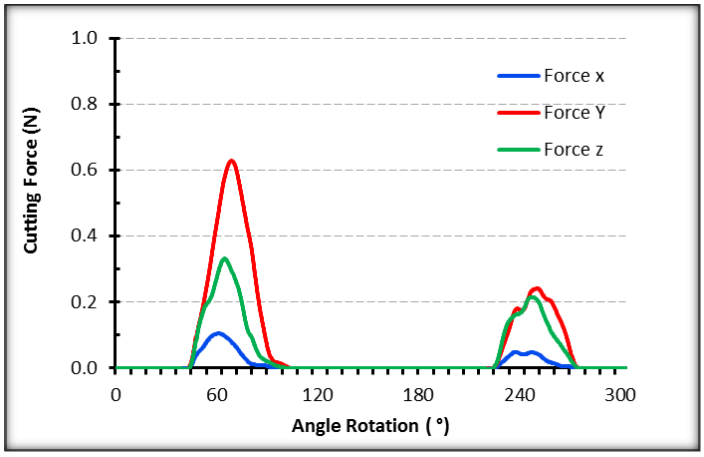

Figure 10: Simulated of cutting force with constant n = 500 rpm, f_t = 0.15mm/flute, Coulomb Friction μ = 0.5.

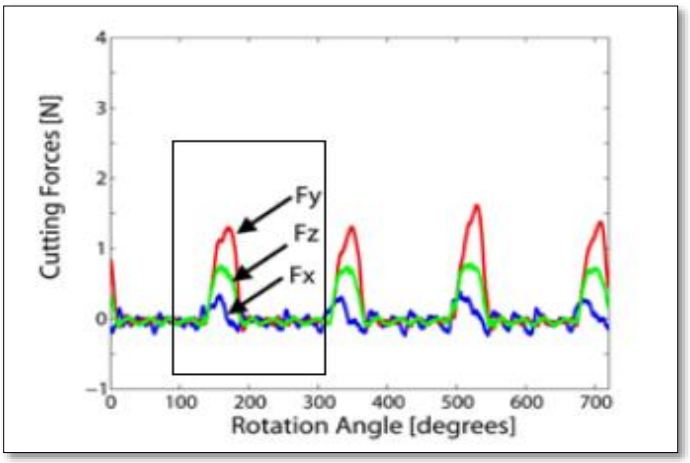

Figure 11: Cutting force captured by force dynamometer with constant n = 500 rpm, f = 2.5 mm/s, f_t = 0.15mm/flute (Graham et al., 2014).

This force deviation could be due to the friction model used in the simulation setup where the simulation only considers the sliding friction using Coulomb friction model only as what been applied by the previous researcher (Davoudinejad et al., 2017; G. Li et al., 2021). As been discussed by (Wang et al., 2020) in his work on the characterization of the coefficient of friction of Aluminum Alloy 6061-T6 constant cutting speed of 500mm/min found that measured friction coefficients ranged from 0.85 to 1.06 over a time, which is slightly higher than the static friction coefficient

between steel and aluminum alloy (Figure 12a). This is also supported by another researcher (S. Li et al., 2021) that found that the coefficient of friction varies with the change of cutting speed and feed rate. The coefficient of friction μ tends to decrease with the increasing cutting speed and feed per tooth ranging from 50 to 300m/min and 0.04 to 0.24mm/rev respectively (figure 12b). Meanwhile, other findings (Grzesik, 2017) state aluminum machining with HSS tools with large positive rake angle, could have values of the mean coefficient of friction, μ reach up to 1.5.

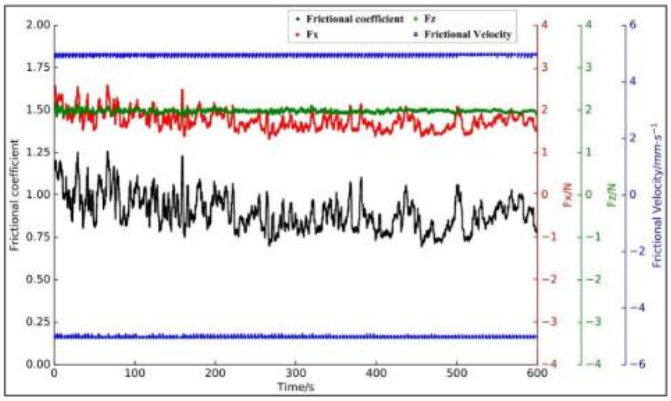

(a)

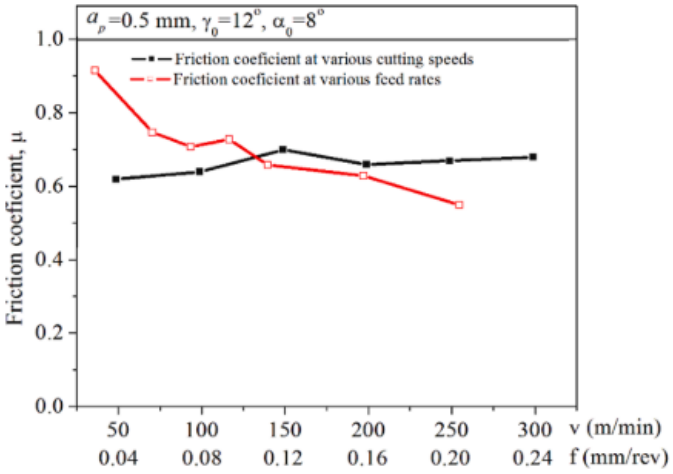

(b)

Figure 12: Coefficient of friction study of Aluminum 6061-T6 materials (a) with constant cutting speed, (Wang et al., 2020) (b) Coefficient of friction dependent on cutting speed and feed per tooth (S. Li et al., 2021).

Another research work on comparative study done by (Kılıçaslan, 2009) seem contradict with the previous work. The comparative study investigates capability of different material and friction models to simulate the cutting operation on AISI 1045 steel material using ABAQUS software. In the study, three common friction model including shear, sliding and hybrid friction models and the comparative results reveal that each of friction model used in the simulation are capable to predict the cutting force although the value are different for each specific friction model. Which

means in the simulation, with appropriate value any of friction model capable to simulate and predict the cutting parameter accurate.

Based on this, all three model has been tested to simulate the inclined dimple milling of Aluminum alloy 6061-T6 and the best result that close fit to the experimental result done (Graham et al., 2013) is by using shear friction model with friction factor, m = 1.05.

3.2 Re-simulation Result

In the re-simulate work, the shear friction model was used to obtain the cutting force and again compared with the actual force captured by experimental work. The graph in figure 13 shows the cutting force endured in all axes during the simulation. Based on the graph force versus angle rotation of tool marked the maximum force in the x, y, and z-axis as 0.15, 0.98 and 0.59 N respectively. Furthermore, the highest force was endured by the y-axis, followed by the z-axis and x-axis, and the ranking of force find good agreement with the experimental result (Graham et al., 2013).

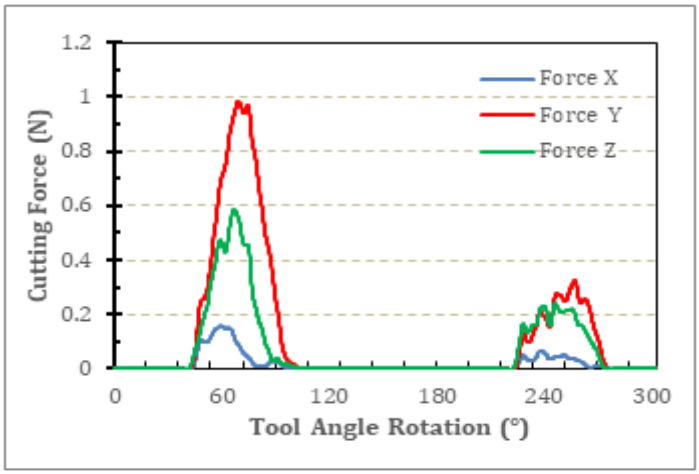

Figure 13; Cutting force gain from the simulation result with constant = 500 rpm, Feed = 0.15mm/flute, Shear Friction Model with m = 1.05.

3.3 Chip Formation

Based on the simulation results using BEM with R_c= 5µm, it is observed that the dimple depth of 7 µm succesfully cut by the first flute and the chip are formed (Figure 14a-f). During cutting, the workpiece material is suppressed in the up-ward direction and then the machining chips are generated since the "uncut chip thickness" is greater than the "minimum chip thickness" according to (Zhang et al., 2019). Further forward, the cutting edge moving beyond the dimple edge causing the formed chip strech-up untill the excessive strain localize at the dimple edge and chip break-off (Figure 14d). For the BEM with R_c= 5µm, the maximum chip thickness measured at 0.01685 mm as shown in figure 14e. In certain machining condition (mainly with R_c>5μm) the formed chip strech-up but did not break-off and tend to remain at the end of the dimple profile. As the chip stick to the dimple edge, causing the burr measuring become more difficult since hard to distinguish between the formed chip and burr.

Furthermore, the following flute mostly ploughing the machined surface of the dimple profile cut by the first flute without forming any chip as shown in figure 14f. This ploughing action by the

cutting tool edge has give straightening effect to the machined dimple surface thus affecting the final surface area roughness of the machined dimple profile as well as promoting residual stress build-up (Zhang et al., 2019) consequently affecting the micro hardness of machined dimple surface (Biondani & Bissacco, 2019).

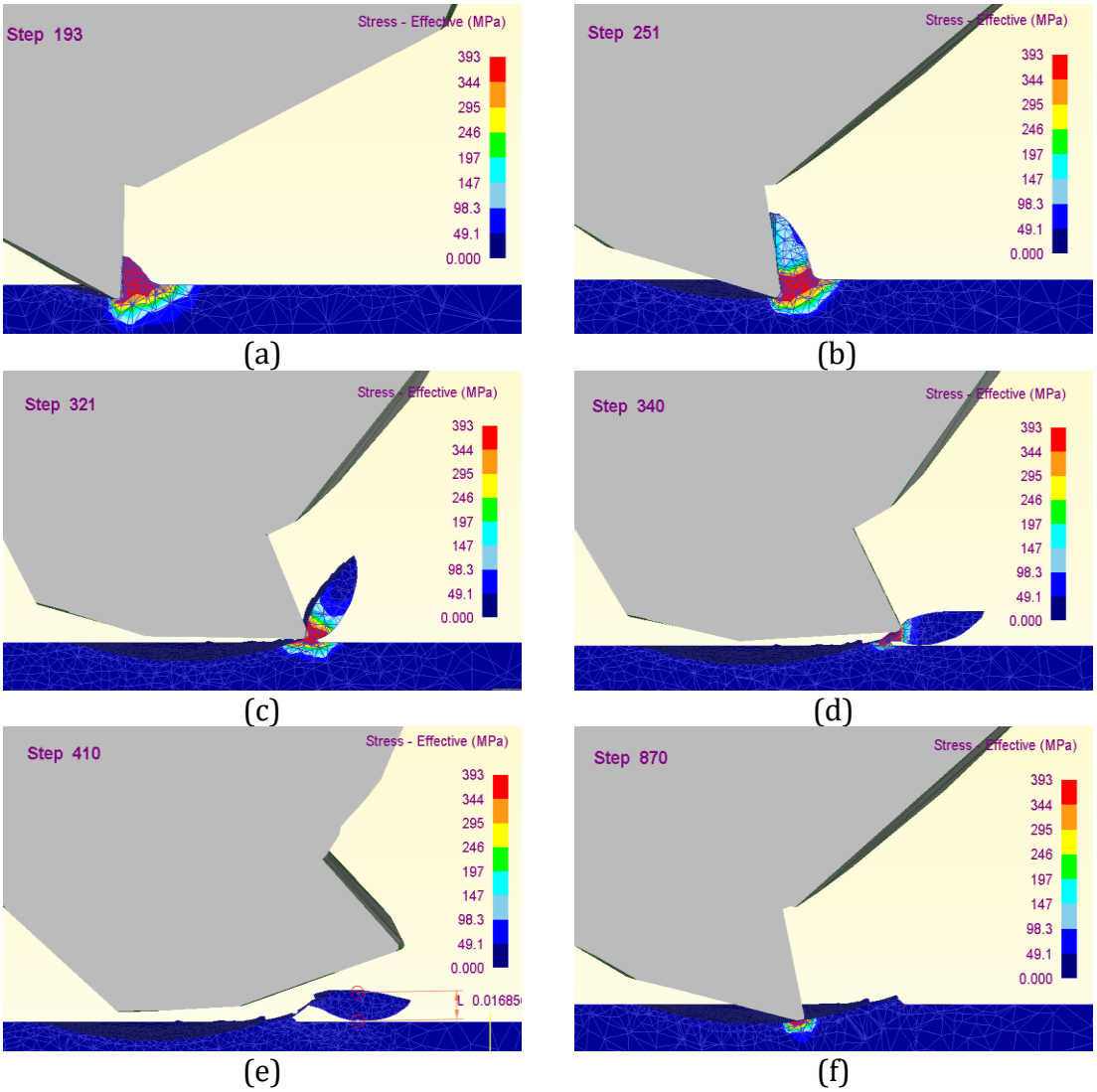

Figure 14(a-f): Cross section view of chip formation sequence in inclined dimple milling with R_c=5µm and dimple depth of 7µm.

3.4 Burr Formation

Based on the simulation results, the burr formation at the dimple edge can be observed and analyzed clearly. The typical build-up burr in inclined dimple milling consists of two elements: Poisson burr and the exit burr. According to (Zhang et al., 2019) the formation of the Poisson burr is due to the stress build-up within the workpiece material as the tool edge penetrates. As the tool

edge penetrates through, the stress build-up not only on the inside of the tool edge trajectory side but on the outside as well (Figure 15a). On the inside, the stress exerted by the tool suppressed the workpiece material in the up-ward direction consequently forming the chip (Figure 15b). While at the outside, as the tool edge approaches the exit edge, the stress exerts by the tool suppressed material in the up-ward direction has caused the workpiece material displacement along the dimple edge thus forming the Poisson burr. Based on the simulation result, the Poisson burr has raised the dimple edge about 0.002 mm.

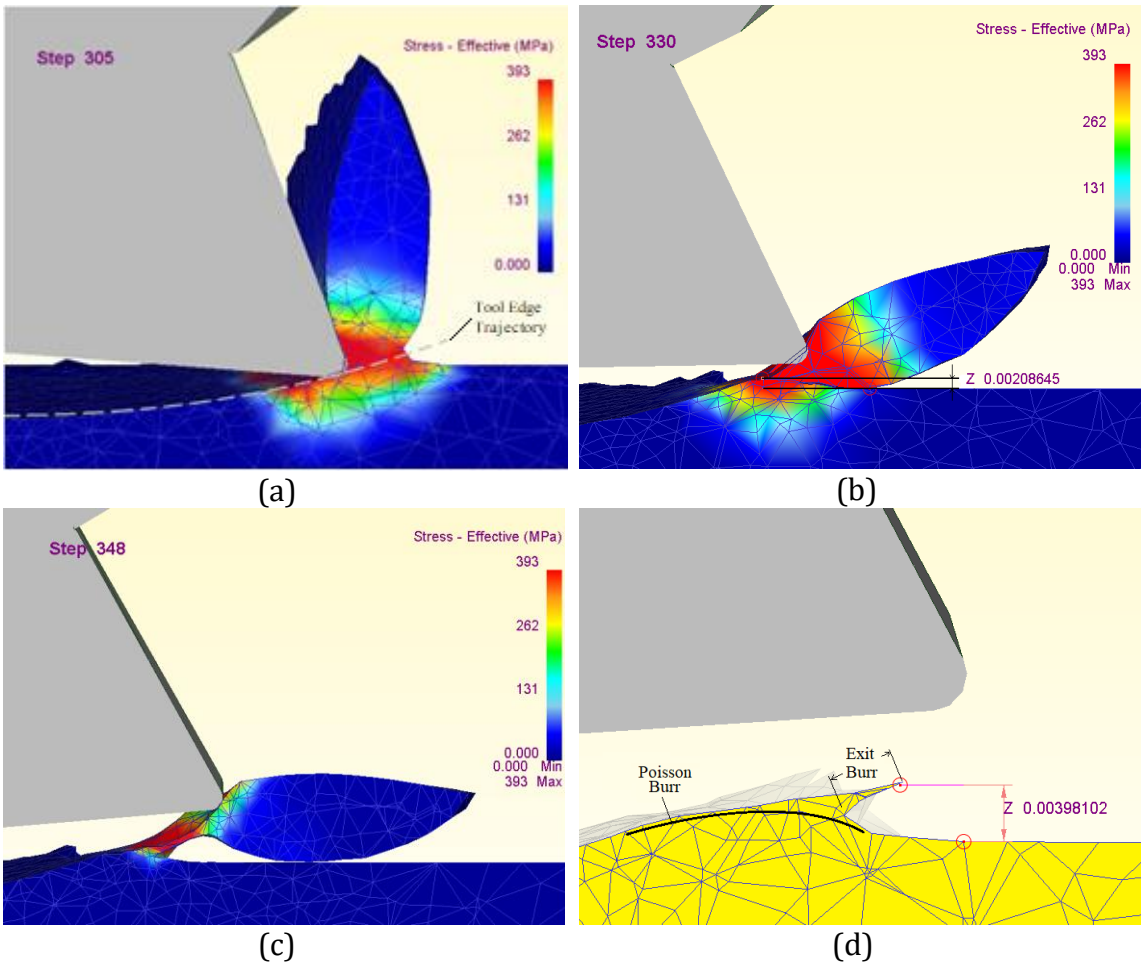

Figure 15 (a-d): Cross section of workpiece shows the stress induced causing the Poisson burr and exit burr formation during dimple machining using BEM with R_c=5µm and dimple depth of 7µm.

Meanwhile the other elements of the build-up burr in inclined dimple milling are the exit burr. As the tool edge passing beyond the dimple edge, the tool edge push forward the chip causing an excessive strain to occur at the chip edge (Figure 15c). As the strain localizes, the chip break-off from the parent workpiece material leaving a rugged protruding edge so called the exit burr as shown in figure 15d below and total burr height (Poisson and exit burr) in z axis direction

measured at 0.004 mm. As predicted, both burr formations occurred at the tool exit side with different width scale (Figure 16a-b). The Poisson burr tends to occur along the dimple edge on the tool exit side with a wider width while the exit burr only occurs at smaller portion on the Poisson burr. In terms of height, Poisson burr contribute almost half of the total burr height while the other half contribute by the exit burr.

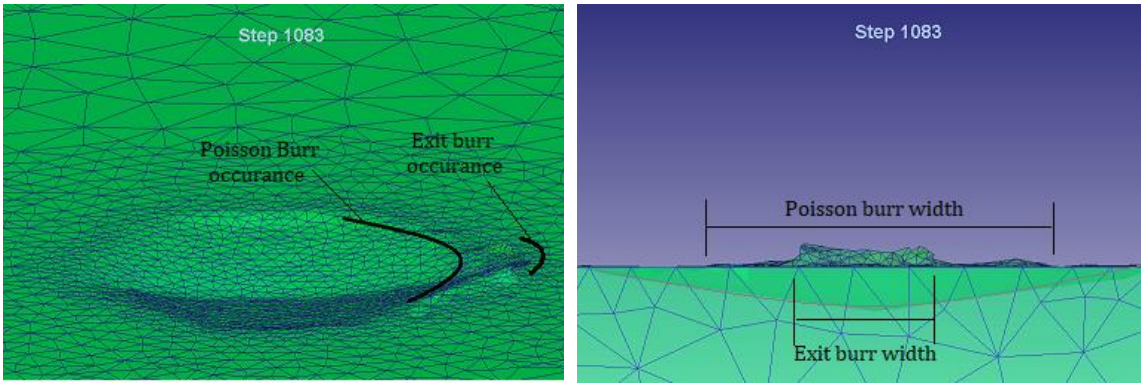

(a) (b)

Figure 16:Location occurance and width comparison between the (a) Poisson burr and (b) Exit burr.

3.5 Result on Effect of Cutting Edge Radius Simulation

A virtual experiment has been setup to study the effect of cutting-edge radius, R_c to the formation of burr on the machined dimple profile. In the study, four different BEM tool model with different R_c ranging from 5 to 30 µm being tested and the result data tabulate in the table 5.

Table 5: Result of burr measurement for the effect of cutting-edge radius, R_c simulation.

Cutting edge radius	Max. Burr Height (µm)	Max. F_y (N)
R_c = 5 µm	3.5 (chip break-off)	0.979
R_c = 10 µm	21.1 (chip not break-off)	0.698
R_c = 20 µm	23.6 (chip not break-off)	0.769
R_c = 30 µm	24.6 (chip not break-off)	0.834

CONCLUSIONS

In this paper, a finite element (FE) simulation approach has been conducted mainly to investigate the cutting force in the inclined dimple milling operation and effect of the BEM cutting-edge radius, R_c to the burr formation. With initial value gain from the literature work, a FE simulation has been conducted and verified with an actual experimental work by comparing the cutting force experienced by the tool-workpiece in all axes. Based on the results gained in the validation has successful determined the approximate value of the coefficient of friction, μ. With that friction coefficient and friction factor, the effect of the BEM cutting-edge radius, R_c to the burr formation has successfully conducted and analyzed. By referring to the simulation results:

1. Friction coefficient, μ of and friction factor, m plays a significant role in influencing the cutting force exerts by the tool-workpiece in the inclined dimple milling simulation as it

been discussed by (Kılıçaslan, 2009) where the increase in friction force will accelerate more heat energy thus soften the workpiece material and indirectly reduce the force.

2. The BEM cutting edge radius, R_c directly affect the cutting force and the burr formation in a way where at micro level, larger radius has a negative rake effect that alter the shear-deformation zone in the workpiece materials (Wan & Cheng, 2013).
3. Burr formation in inclined dimple milling is inevitable due to the stress formation within the workpiece materials but could be minimize with optimized parameters such as cutting speed, feed, rake angle and cutting-edge radius, R_c (Grzesik, 2017) as well as other possible method such using support materials (Wan, 2013) .

Based on the drawn conclusion, it seems like a lack of authentication of work due to the limitation of experimental data. So, in the future work should work out on several areas mainly on conducting an experimental work so that validation of chip shape and burr shape formed in the simulation with actual machined chip could be conducted to improve the simulation reliability. One last critical point on simulation work, a thoughtful measure should be taken in term of determining an actual Friction coefficient, μ of and friction factor, m using experimental approach to ensure the reliability and repeatability of the gathered data.

ACKNOWLEDGEMENT

This research paper is part of author doctoral research work and authors gratefully acknowledge the financial support by Universiti Malaysia Pahang (UMP) under Post Graduate Research Scheme (PGRS200324).

REFERENCES

Biondani, F. G., & Bissacco, G. (2019). Effect of cutting edge micro geometry on surface generation in ball end milling. CIRP Annals, 68(1), 571–574. https://doi.org/10.1016/j.cirp.2019.04.017.

Bolar, G., & Joshi, S. (2014, December 12). 3D finite element modeling of thin-wall machining of aluminum 7075-T6 alloy. 5th International & 26th All India Manufacturing Technology, Design and Research Conference (AIMTDR 2014).

Chen, Z., Qin, L.-F., & Yang, L.-J. (2015, January 1). Cutting Force Simulation of Titanium based on DEFORM-3D. Conference: 3rd International Conference on Material, Mechanical and Manufacturing Engineering (IC3ME 2015). https://doi.org/10.2991/ic3me-15.2015.356.

Chen, W., Teng, X., Zheng, L., Xie, W., & Huo, D. (2018). Burr reduction mechanism in vibration-assisted micro milling. Manufacturing Letters, 16, 6–9. https://doi.org/https://doi.org/10.1016/j.mfglet.2018.02.015

Chen, Z., Wu, X., Zeng, K., Shen, J., Jiang, F., Liu, Z., & Luo, W. (2021). Investigation on the Exit Burr Formation in Micro Milling. Micromachines, 12, 952. https://doi.org/10.3390/mi12080952

Childs, T. H. C. (2006). Friction modelling in metal cutting. Wear, 260(3), 310–318. https://doi.org/https://doi.org/10.1016/j.wear.2005.01.052

Davoudinejad, A., Parenti, P., & Annoni, M. (2017). 3D finite element prediction of chip flow, burr formation, and cutting forces in micro end-milling of aluminum 6061-T6. Frontiers of Mechanical Engineering, 12. https://doi.org/10.1007/s11465-017-0421-6

Graham, E., Park, C. I., & Park, S. S. (2013). Fabrication of micro-dimpled surfaces through micro ball end milling. International Journal of Precision Engineering and Manufacturing, 14(9), 1637–1646. https://doi.org/10.1007/s12541-013-0221-9

Graham, E., Park, C. I., & Park, S. S. (2014). Force modeling and applications of inclined ball end milling of micro-dimpled surfaces. International Journal of Advanced Manufacturing Technology, 70(1–4), 689–700. https://doi.org/10.1007/s00170-013-5310-5

Grzesik, W. (2017). Chapter Eleven - Tribology of Metal Cutting. In W. Grzesik (Ed.), Advanced Machining Processes of Metallic Materials (Second Edition) (pp. 197–214). Elsevier. https://doi.org/https://doi.org/10.1016/B978-0-444-63711-6.00011-9

Ji, W., Liu, X., Wang, L., Meng, Y., & Wu, X. (2015). A study on geometry modelling of a ball-end mill with chamfered cutting edge. Journal of Manufacturing Processes, 19, 205–211. https://doi.org/https://doi.org/10.1016/j.jmapro.2014.10.003

Kiswanto, G., Zariatin, D. L., & Ko, T. J. (2014). The effect of spindle speed, feed-rate and machining time to the surface roughness and burr formation of Aluminum Alloy 1100 in micro-milling operation. Journal of Manufacturing Processes, 16(4), 435–450. https://doi.org/10.1016/j.jmapro.2014.05.003

Kılıçaslan, C. (2009). Modelling of metal cutting by finite element method.

Li, G., Liu, M., & Zhao, S. (2021). Reduced computational time in 3D finite element simulation of high speed milling of 6061-T6 aluminum alloy. Machining Science and Technology, 25(4), 558–584. https://doi.org/10.1080/10910344.2020.1855651

Li, S., Sui, J., Ding, F., Wu, S., Chen, W., & Wang, C. (2021). Optimization of Milling Aluminum Alloy 6061-T6 using Modified Johnson-Cook Model. Simulation Modelling Practice and Theory, 111, 102330. https://doi.org/https://doi.org/10.1016/j.simpat.2021.102330

Luo, M., Liu, G., & Chen, M. (2008). Mechanism of burr formation in slot milling Al-alloy. International Journal of Materials and Product Technology, 31(1), 63–71.

Lv, D., Wang, Y., & Yu, X. (2020). Effects of cutting edge radius on cutting force, tool wear, and life in milling of SUS-316L steel. The International Journal of Advanced Manufacturing Technology, 111(9), 2833–2844. https://doi.org/10.1007/s00170-020-06286-7

Mohruni, A. S., Zahir, M., Yanis, M., Sharif, S., & Yani, I. (2019). Investigation of Finite Element Modelling on Thin-Walled Machining of Ti6Al4V using DEFORM-3D. Journal of Physics: Conference Series, 1167, 012002. https://doi.org/10.1088/1742-6596/1167/1/012002

Pratap, T., & Patra, K. (2018). Micro ball-end milling—an emerging manufacturing technology for micro-feature patterns. International Journal of Advanced Manufacturing Technology, 94(5–8), 2821–2845. https://doi.org/10.1007/s00170-017-1064-9

Saptaji, K., Subbiah, S., & Dhupia, J. S. (2012). Effect of side edge angle and effective rake angle on top burrs in micro-milling. Precision Engineering, 36(3), 444–450. https://doi.org/https://doi.org/10.1016/j.precisioneng.2012.01.008

Tamizharasan, T., & Senthilkumar, N. (2012). Optimization of Cutting insert geometry using DEFORM-3D: Numerical Simulation and Experimental Validation. International Journal of Simulation Modelling, 11, 65–76. https://doi.org/10.2507/IJSIMM11(2)1.200

Usui, E., & Takeyama, H. (1960). A photoelastic analysis of machining stresses.

Vipindas, K., Anand, K. N., & Mathew, J. (2018). Effect of cutting edge radius on micro end milling: force analysis, surface roughness, and chip formation. The International Journal of Advanced Manufacturing Technology, 97(1), 711–722. https://doi.org/10.1007/s00170-018-1877-1

Wan, Y. (2013). An innovative method for surface defects prevention in micro milling and its implementation perspective. Proceedings of the Institution of Mechanical Engineers, Part J: Journal of Engineering, 227, 1347.

Wan, Y., & Cheng, K. (2013). An investigation on the tool cutting edge radius and “boundary effect” on burr formation and control in micromilling. Laser Metrology and Machine Performance X -

10th International Conference and Exhibition on Laser Metrology, Machine Tool, CMM and Robotic Performance, LAMDAMAP 2013, 341–350. https://www.scopus.com/inward/record.uri?eid=2-s2.0-84908274941&partnerID=40&md5=e89fa7ecb2875976c533ee567066fcab

Wang, H., Zhang, T., Wang, S., & To, S. (2020). Characterization of the Friction Coefficient of Aluminum Alloy 6061 in Ultra-Precision Machining. Metals, 10, 336. https://doi.org/10.3390/met10030336

Yıldız, A., Kurt, A., & Yağmur, S. (2020). Finite element simulation of drilling operation and theoretical analysis of drill stresses with the Deform-3D. Simulation Modelling Practice and Theory, 104, Article No: 102153. https://doi.org/10.1016/j.simpat.2020.102153

Zhang, X., Yu, T., Wang, W., & Zhao, J. (2019). Improved analytical prediction of burr formation in micro end milling. International Journal of Mechanical Sciences, 151, 461–470. https://doi.org/https://doi.org/10.1016/j.ijmecsci.2018.12.005

Zorev, N. N. (1963). Inter-relationship between shear processes occurring along tool face and shear plane in metal cutting. ASME, New York, 42–49.